IEEE Access
Multidisciplinary ⋮ Rapid Review ⋮ Open Access Journal

Received May 22, 2021, accepted June 9, 2021, date of publication June 16, 2021, date of current version July 6, 2021.

Digital Object Identifier 10.1109/ACCESS.2021.3089895

A Metamaterial Absorber Based on Particle Swarm Optimization Suitable for Earth's Atmospheric Transparency Window

JING LIU[1], WEN-ZHUANG MA[1], WEI CHEN[2], YU-SHAN CHEN[1], XU-CHU DENG[1], AND YU GU[1]

[1]School of Ocean Information Engineering, Jimei University, Xiamen 361021, China
[2]Navigation Institute, Jimei University, Xiamen 361021, China

Corresponding authors: Wei Chen (weichen@jmu.edu.cn) and Yu Gu (guyufrankfurt@163.com)

This work was supported in part by the Fujian Provincial Department of Science and Technology under Grant 2019H0022, in part by the Science Fund for Distinguished Young Scholars of Fujian Province under Grant 2020J06025, in part by theYouth Talent Support Program of Jimei University under Grant ZR2019002, in part by the Innovation Fund for Young Scientists of Xiamen under Grant 3502Z20206021, in part by the Xiamen Marine and Fishery Development Special Fund under Grant 20CZB014HJ03, in part by the Fujian Provincial Natural Science Foundation under Grant 2020J01712, and in part by the Youth Talent Support Program of Fujian Province (Eyas Plan of Fujian Province) [2021].

ABSTRACT The absorption and reflection of electromagnetic waves by various particles in the earth's atmosphere allow the passage of only certain electromagnetic wavelengths to reach the ground, called Earth's atmosphere transparent window. In this study, perfect absorption was theoretically obtained in the range of near- and mid-infrared earth's atmospheric transparency window using a simple absorber with metal-dielectric-metal structure. The numerical simulations showed the average absorption to reach 96.2% at wavelengths from 2000 to 6000 nm. Also, the broadband absorption was noticed and attributed to combined physical mechanisms, such as anti-reflection effect, localized surface plasmon polariton, propagating surface plasmon polarization, Fabry–Pérot cavity and slow light mode. Meanwhile, the proposed absorber displayed simple-structure, low-cost, wide-angle, and polarization-independent. In sum, the proposed absorber might be useful for future applications related to atmospheric transparency window, such as remote sensing, energy harvesting, infrared detection, and stray light elimination.

INDEX TERMS Metamaterials, perfect light absorption, surface plasmon, earth's atmospheric transparency window.

I. INTRODUCTION

Perfect absorbers (PA) based on metamaterials have been the subject of intensive research in recent years owing to their various potential applications in infrared stealth, daytime radiative cooling, solar energy, and thermal imaging, among others [1]–[9]. In 2008, Landy *et al.* reported the first metamaterial PA functioning in the gigahertz (GHz) range [10]. Today, the rapid development of optical simulations based, for instance, on rigorous coupled-wave analysis and finite difference time domain (FDTD) coupled to modern manufacturing processes like additive manufacturing and micro-nano processing, led to enlarged absorption ranges of PAs from radio frequency (RF) to optical spectra, including ultraviolet, visible, infrared, microwaves and radio waves [11]–[14]. Note that all substances above the absolute zero (−273 °C) could generate infrared light. In particular, infrared corresponding to wavelengths from 2 to 2.6 μm and 3 to 6 μm or referred to as near- and mid-infrared atmospheric transparency window (ATW), has received increasing interest [15]. The reason for this has to do with the portion of this wavelengths, which may pass through the earth's atmosphere with little loss or distortion. This makes infrared atmospheric transparency window devices useful for applications related to atmospheric transparency window, such as remote sensing, energy harvesting, radiative cooling, infrared detection, and stray light elimination [16]–[19].

According to Wien's displacement law, the near-infrared (NIR) and mid-infrared (MIR) located in the thermal infrared remote sensing working range and sensitive to

The associate editor coordinating the review of this manuscript and approving it for publication was Yee Sin Ang.

high-temperature target recognition like fires and active volcanoes, could effectively capture high-temperature information available on the ground. This can be explained through the relationship: $\lambda_m T \approx 2.9 * 10^{-4} m \cdot k$, with maximum radiation for absolute temperatures of $T = 1450$ and 485 k occurring at $\lambda = 2000$ and 6000 nm, respectively. In this view, demand for broadband high absorption associated with this wavelength band has quickly risen in recent years.

On the other hand, previous studies have focused on the use of multilayered structures consisting of alternating layers of flat metal and dielectric plates as common infrared absorbers. The reason for this has to do with nature of the structure, which could broaden the absorption bandwidths [20], [21]. For instance, Cui *et al.* theoretically proposed a metamaterial PA with 20 metal-dielectric (M-D) layers, and predicted absorptions above 95% in the spectral range from 3000 to 5500 nm [16]. Deng *et al.* experimentally prepared a 13-pair M-D multilayer absorber with broadband high absorption from 1000 to 6000 nm [22]. However, despite the broadband infrared light absorption of these absorbers, their fabrication methods rely on multiple costly nanofabrication processing steps and precise manufacturing, such as focused ion beam, electron-beam lithography and high-resolution photolithography [23]. Moreover, the polarization angle and incident angle could vary during practical applications, and thereby require consideration. This makes the design of infrared absorbers more challenging, especially infrared ATW absorbers.

To overcome these issues, various infrared absorbers have been designed and tested. For instance, Yu *et al.* reported a broadband plasmonic absorber for mid-infrared ATW based on metal–spheres–metal–insulator–metal structure with high absorption of 90% from 3000 to 6000 nm [18]. However, though this absorber ideally covers absorptions in the MIR ATW range, the construction of the metal–spheres–metal–insulator–metal structure remains complex and costly since gold has been used. Therefore, the design of ATW absorbers with ideal broadband absorption, low-cost, and simple fabrication process is still challenging.

On the other hand, incident light on metal surfaces should reflect, thereby reducing the absorption of structures [24]. To overcome the problem, antireflection (AR) coatings have been used in some schemes to reduce the reflection of incident light. For example, Yang *et al.* demonstrated the benefit of AR coatings in achieving optical admittance locus matching between the absorber and free space [25]. AR coatings have also been applied as significant optical materials in IR region in many optoelectronic systems requiring suitable AR coatings to enhance the transmission. In this view, high bandgap perovskite absorbers have shown up to 30% tandem efficiency when tested by photoluminescence quantum yield analysis, which can be achieved by adapting charge transport materials and surface passivation along with improved AR measures [26]. Thus, appropriate AR coatings should improve the absorption efficiencies.

Furthermore, the rapid development of machine learning based on various efficient optimization algorithms has started to widespread to other disciplines, such as physics, materials science, and biology [27]. *Cai et al.* designed an ultra-broadband near-perfect bilayer grating metamaterial absorber using genetic algorithm method with maximized average absorption range from 300 to 2100 nm [28]. Tao *et al.* employed particle swarm optimization (PSO) to predict the chiral optical response of two-dimensional chiral metamaterials [29]. Thus, an optimization algorithm is required for improved structural design.

Herein, a simple metal-dielectric-metal (MDM) structure with omnidirectional and broadband absorption across ATW spectrum was described for the first time. The as-obtained absorber was further optimized by PSO algorithm and AR effect. The top MgF_2 layer acted as AR protective coating to enhance the absorption performance and protect the metal from oxidation or corrosion. The average absorption over the range of 2000-6000 nm reached 96.2%. Furthermore, the recorded high absorption was completely independent of light polarization and was maintained even at large incident angles of oblique incidence up to 60 degrees. The calculated distributions of charge and current density, absorbed power, electric field, magnetic field, Poynting vector, and numerical simulations all linked the broadband absorption effect to multiple physical mechanisms. In sum, the proposed absorber showed numerous excellent characteristics, including simultaneous ultra-broad and perfect absorption performances, low cost, and simple fabrication. Such a MDM structure would be useful for the construction of perfect absorbers for ATW with extremely simple designs.

II. GEOMETRY, PARAMETERS, AND METHODS

The schematic diagram and cross-section of the proposed absorber are provided in Fig. 1(a) and 1(b). A Fe square covering MgF_2 coating was supported by TiO_2-Fe layer. The absorber exhibited polarization-independent characteristics thanks to the symmetry of the structure. Strong and confined near field may be generated in the nanogap between adjacent metal patches. MgF_2 layer was not only used as an anti-corrosion coating to prevent iron from oxidation but also as an AR coating. Compared with the most commonly used noble metal in metamaterials, the Fe is much more beneficial for realizing impedance matching over a broad frequency band in near-infrared range. At the same time, the applying of the Fe in a metamaterial absorber may greatly reduce the production cost in application [30]. The average refractive index of TiO_2 in the atmospheric window band is about 2.3. The different metals and media are compared in later sections of this paper. The bottom Fe layer was used as backside reflector and was thicker than skin depth of the infrared light range to prevent transmission of the incident light. Therefore, the absorption can be represented by the formula: $A = 1 - R$, where A and R are respectively the absorption and reflection. Moreover, the bottom Fe layer produced a Fabry–Pérot cavity together with the top layer and dielectric layer. Thus, reflected

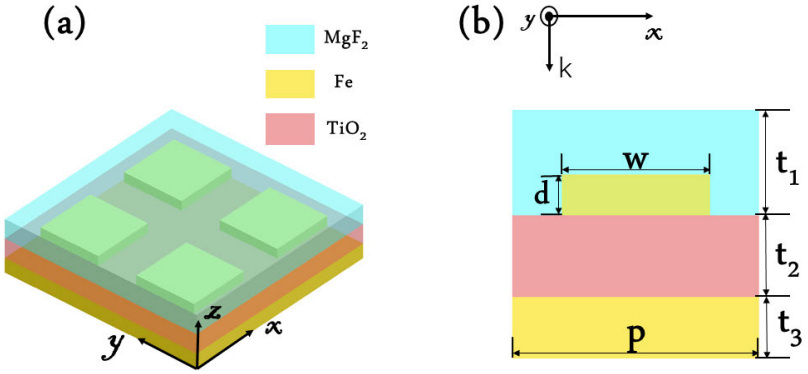

FIGURE 1. Schematic diagram (a) and cross-section (b) of a unit cell the proposed absorber.

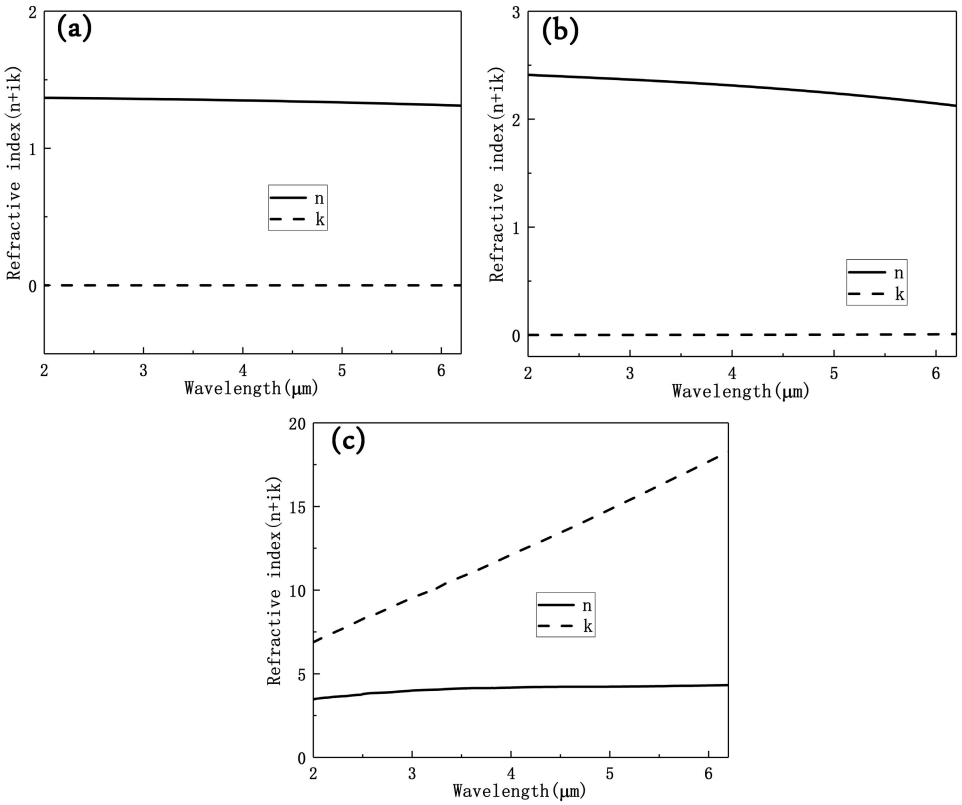

FIGURE 2. The refractive index of (a) MgF_2, (b) TiO_2 and (c) Fe.

energy could be suppressed by ohmic losses in Fe patches, which will be shown later.

The related geometry parameters of the unit cell are provided in Fig. 1(b). As shown in Fig. 2, the optical parameters of MgF_2, TiO_2 were taken from references [31], [32], and Fe, Au were taken from CRC Handbook of Chemistry & Physics [33]. The proposed structure was calculated by electromagnetic full-wave FDTD method and optimized by PSO algorithm. For FDTD simulations, the periodic boundary conditions were set along the x- and y-axis, and perfectly matched layer boundary conditions were employed along the z-axis [34]. A vertical incident TM light was utilized as incident light along the negative z-direction, and polarization of the incident light was directed along the x-direction. PSO was derived from the study of predatory behaviour of birds, aiming to search for optimal solutions through cooperation and information sharing among individuals in a group. Firstly, PSO randomly generated each particle with different structural parameters within a specified range. Next, FDTD method was used to calculate the average absorption of each particle at wavelengths from 2000 nm to 6000 nm.

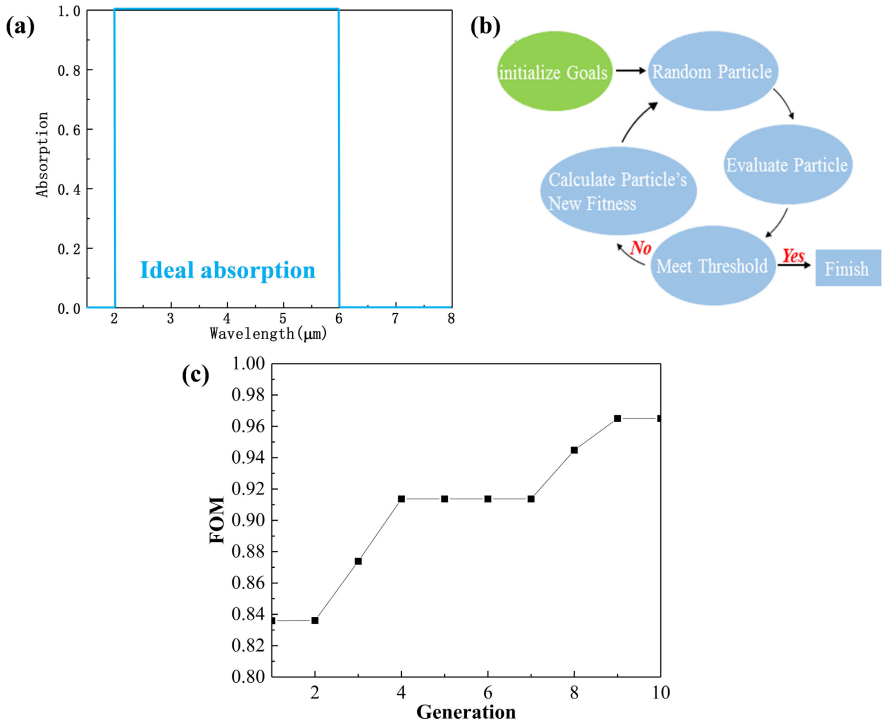

FIGURE 3. (a) The diagram of optimal absorption. (b) The flow diagram of PSO. (c) Optimal average absorption per generation.

The diagram of optimal absorption and flow diagram of PSO are depicted in Fig. 3. The average absorption was calculated according to the formula: $A = \int_{\lambda 1}^{\lambda 2} A(\lambda)\, d\lambda/(\lambda_1 - \lambda_2)$, where λ_1 and λ_2 are respective wavelengths at 6000 and 2000 nm. The optimal average absorption (figure of merit, FOM) was set to 1. The maximum number of iterations was set to 30 generations (each generation being 20 parameters). Both the calculated and optimal values were then substituted into a fitness function, and the optimization process ended when the maximum number of iterations was reached or the optimal average absorption was satisfied. If not, the particles will update their positions according to the fitness function. The proposed optimization process was then repeated until the standard stopped. More details of PSO can be found in the literature [28]. As shown in Fig. 3c, when iterating to the ninth layer, the FOM no longer changes and the optimal structural parameters are obtained. The structural parameters optimized according to the above PSO are shown in Table 1.

According to the actual preparation process and structural parameters, we fine-tuned some of the optimized structural parameters to adjacent integers, the optimal parameters were determined as: $p = 400$ nm, $w = 320$ nm, $t_1 = 600$ nm, $d = 10$ nm, $t_2 = 270$ nm, and $t_3 = 100$ nm.

III. RESULTS AND DISCUSSION

The ideal absorption of the proposed structure obtained by PSO and actual preparation technology is depicted in Fig. 4(a). Nearly perfect absorption (over 90%) was achieved at wavelengths from 2120 to 5830 nm. According to calculations, the average absorption rate of the proposed absorber from 2000 to 6000 nm reached 96.2%.

The high absorption rate at wide bandwidth is one of the important indicators for designing an absorber. Considering the practical applications, the designed absorbers must be large incidence angle insensitive and polarization independent. The material and number of layers are directly related to their production cost and manufacturing process, so they also need to be considered. As can be seen in Table 2, our proposed structure can provide a wider absorption bandwidth from 2 to 6 compared to existing ATW absorbers. Most importantly, our proposed absorber is low cost (without precious metals), angle insensitive, polarization independence and has an ultra-thin thickness.

Moreover, the proposed absorber provided an ideal absorption in the entire NIR- and MIR- ATW spectral ranges. To gain a better understanding of the broadband nearly perfect absorption behaviour, the proposed structure was further analysed from various perspectives.

To illustrate the AR effects, the absorption spectrum of the structure containing MgF_2 cap was compared to that without cap under identical parameters. The absorption spectra of both cases are compared in Fig. 4(b). Obviously, the absorption efficiency and bandwidth rose for the structure with MgF_2 cap. Since A = 1-R, MgF_2 cap might be considered as AR coating, which can reduce R and increase A.

TABLE 1. The key structural parameters of the ATW absorber.

Layer no.	Optimized parameter (nm)	Final parameter (nm)
t_1	600	600
t_2	271.3	270
t_3	99.2	100
p	402.9	400
w	318.7	320
d	9.8	10

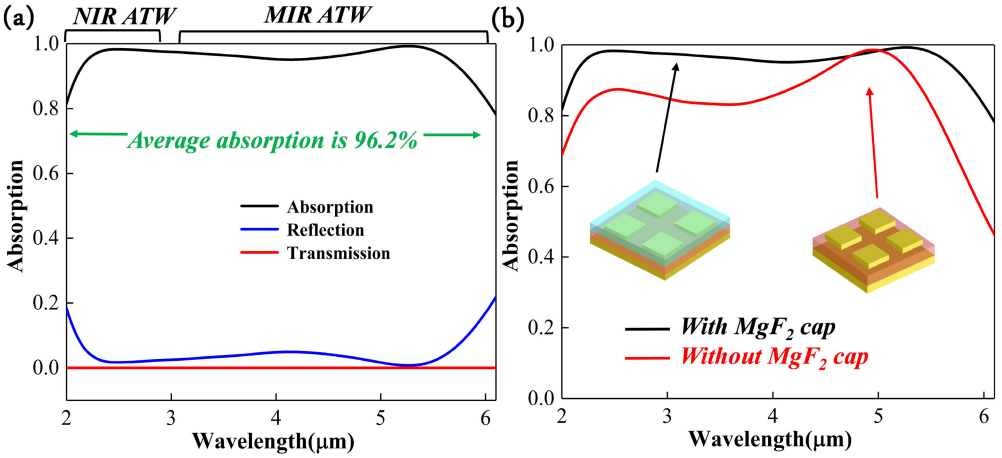

FIGURE 4. (a) Absorption spectrum of the proposed absorber. (b) Absorption spectrum of the structure containing MgF_2 cap (black line) compared to that without cap (red line).

TABLE 2. Comparison of various ATW absorber.

Reference	Bandwidth	Angular Stability	Absorption	Polarization Independent	Materials	Number of Layers
[16]	3-5.5	Up to 60	95%	No	Au, Ge	41
[18]	3-6	Up to 60	90%	Yes	polystyrene spheres	-
[46]	3.5-4.8	-	80%	No	Au, InP	33
[47]	3-5	-	90%	Yes	Al, $Ge_3Sb_2Te_6$	3
This work	2-6	Up to 60	96.2%	Yes	Fe, TiO_2, MgF_2	4

To gain a better understanding of AR effects, the proposed structures were further analysed by impedance matching method and effective medium theory. The relation between impedance Z and S parameters can be expressed as [16]:

$$S_{11} = S_{22} = \frac{i}{2}\left(\frac{1}{Z} - Z\right)\sin(nkd) \tag{1}$$

$$S_{21} = S_{12} = \frac{1}{cos\,(nkd) - \frac{i}{2}(Z + \frac{1}{2})sin(nkd)} \tag{2}$$

where S_{11}, S_{22}, S_{21}, and S_{12} are S parameters and n is the effective refractive index, k is the wave vector, and d is the thickness of designed structure. Thus, the impedance Z can be yielded by:

$$Z = \pm\sqrt{\frac{(1 + S_{11})^2 - S_{21}^2}{(1 - S_{11})^2 - S_{21}^2}} \tag{3}$$

For a perfect absorber, the impedance should match the free-space impedance ($Z = Z_0 = \sqrt{\frac{\mu}{\varepsilon}} = \mathbf{1}$). Fig. 5 gathers the impedance curves and reflection of free spaces for both structures with and without MgF_2 cap. At wavelengths $\lambda = 2460$ and 5480 nm (Fig. 5(f)), the impedance values of the real and imaginary parts were close to 1 and 0, respectively. Besides, a perfect absorption reaching 99.9% was obtained (Fig. 4(a)). Therefore, the proposed absorber

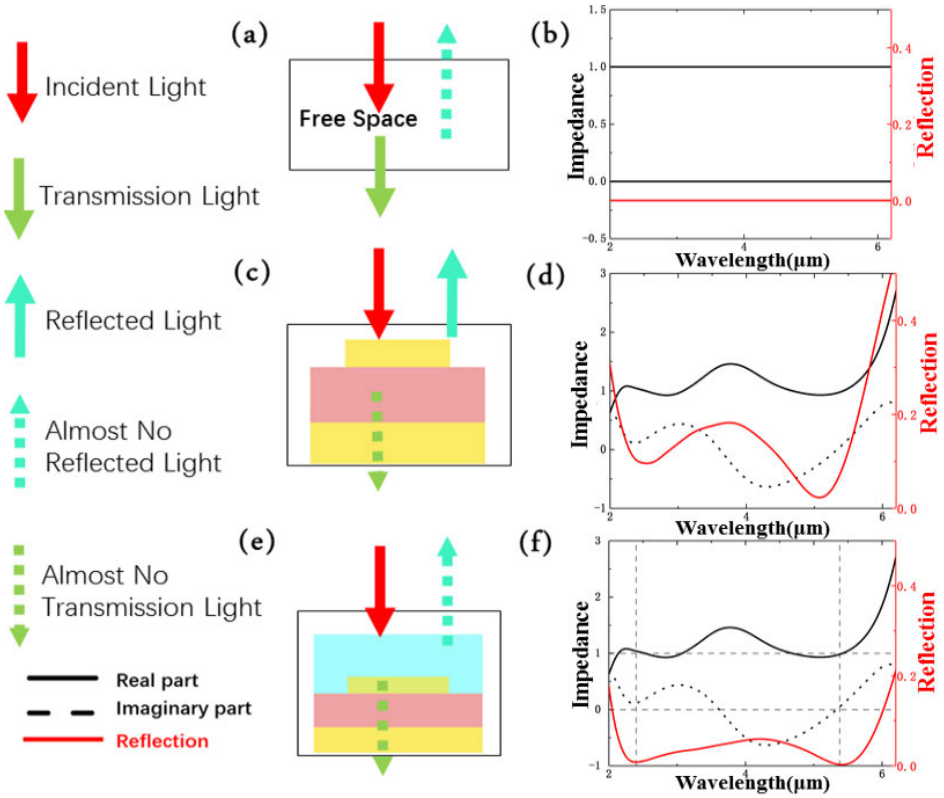

FIGURE 5. Impedance matching scheme of: free space (a), structure without MgF_2 cap (c), and structure with MgF_2 cap (e). Impedance curve and reflection of free space (b), structure without MgF_2 cap (d), and structure with MgF_2 cap (f).

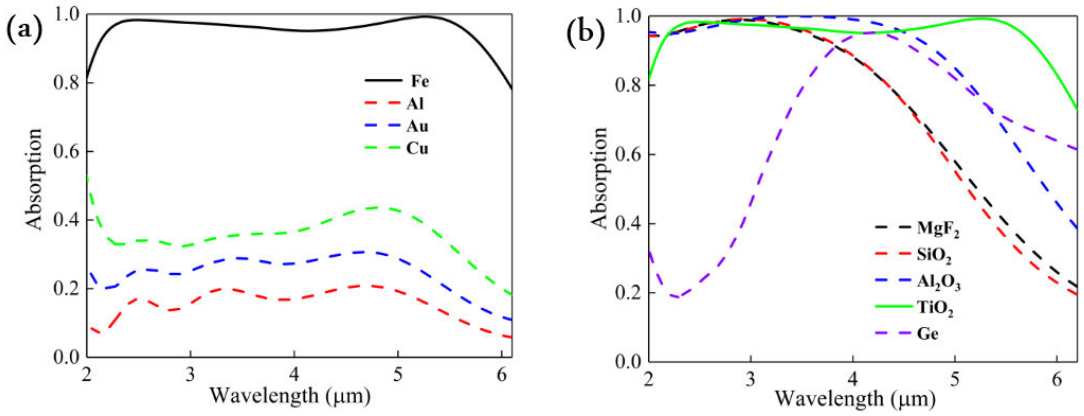

FIGURE 6. (a) Comparison of absorption with different types of the metal. and (b) Comparison of absorbance with different types of the dielectric layer.

possessed a novel device configuration with significantly enhanced absorption efficiency. By exploiting the AR effects, the structure with MgF_2 cap showed decreased reflection by ∼10% when compared that without MgF_2 cap.

Fe is not common to construct the MDM absorber in the infrared spectrum. Next, in order to enrich our work, we simulated the structure of other materials. One can see from Fig. 6(a) that the materials of metal have a key influence on the absorption performance of the proposed structure. When Au, Al or Cu are used as metal layers, the absorption is lower due to their smaller metal loss. Moreover, we compared the absorption performance with different dielectric materials; the results are shown in Fig. 5(a). The new materials are MgF_2, SiO_2, Al_2O_3, and Ge. One can see that TiO_2 is more suitable to obtain better average absorption than the other materials. The reason for this kind of variation is the different refractive indices of those materials. As we know, for visible to near-infrared metamaterial absorbers, the lower

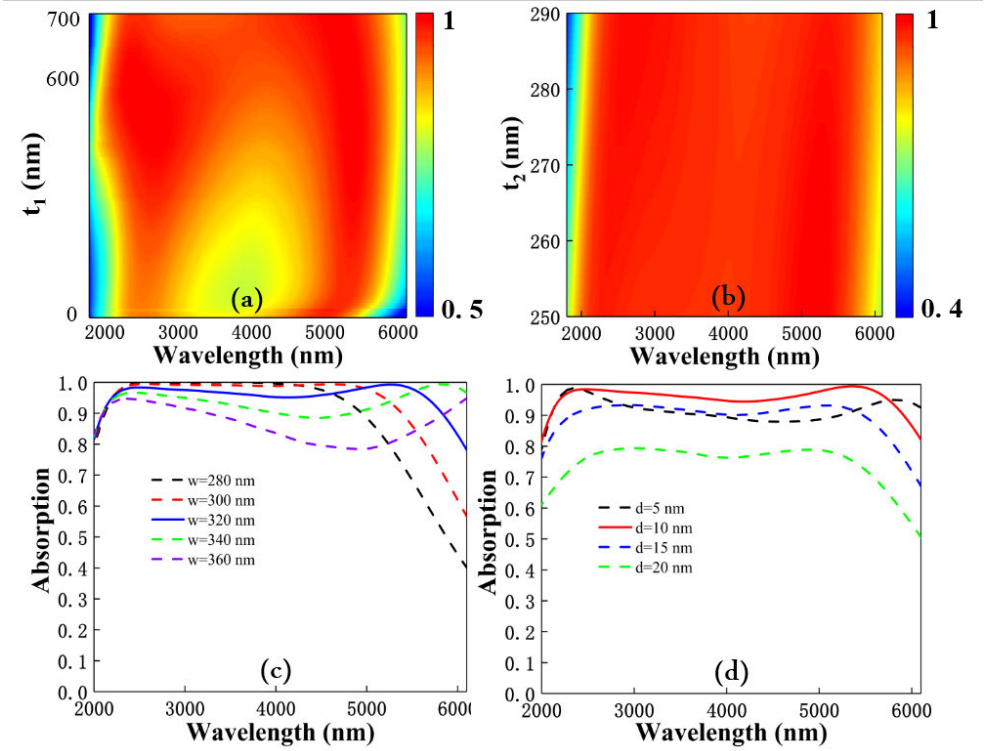

FIGURE 7. Absorption spectra versus different value of (a) "t_1", (b) "t_2", (c) "w", (d) "d".

the refractive index, the higher the absorption and the more extensive the bandwidth [7]. As shown in Fig. 6(b), when the refractive index of the material is smaller than TiO_2 (see Fig. 2(b)), the absorber has better absorption at short wavelengths. Due to the dispersion properties of TiO_2, it achieves better impedance matching at long wavelengths. Thus, Fe and TiO_2 were the most suitable material to obtain a high absorption in the ATW band.

In order to prove the superiority of the structure, we swept the key parameters in Fig. 7. To visualize the AR effect, the thickness t_1 of the MgF_2 cap was recorded as a function of absorption in Fig. 7(a). When t_1 value increases from 0 nm to 700 nm, the absorption of the absorber first increase, reach an optimum value at 600 nm, and then the bandwidth becomes shorter as the t_1 value further increases. The main and important scan with the parameter t_2 takes place here. Here, the thickness of the dielectric layer increases from 250 nm to 290 nm, which is shown to be significant in Fig. 7(b). The bottom and top metals generate capacitance with the help of a dielectric layer. The capacitance of the structure depends strongly on the dielectric thickness and is inversely proportional to the dielectric thickness. As the thickness increases, the capacitance decreases; thus the absorption bandwidth moves linearly from left to right. Also, the dielectric layer confined most of the wave within it and made a structure highly procurable for absorption. Here, when t_2 is equal to 270 nm, the high absorption bandwidth is mainly concentrated in the ATW band. Figure 7(c) illustrates

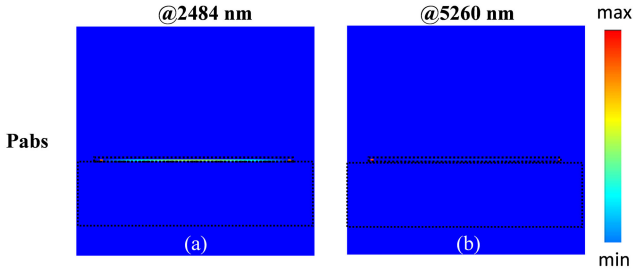

FIGURE 8. Distributions of absorbed power (P_{abs}) at different wavelengths.

the variations of absorption performance as a function of the side length "w" of Fe and the other parameters shown in Fig. 1 were unchanged. When the value of w is small, the absorber has high absorption in the short wavelength band. With the increase of value of w, the absorption peak gradually blue shifts. Here, when w is equal to 320 nm, the high absorption bandwidth is mainly concentrated in the ATW band. As shown in Fig. 6(d), the average absorption in the ATW band of the designed absorber is maximum when the thickness of the top Fe layer (d) is 10 nm. In Fig. 7, the swept spectra confirmed the rationality of PSO since the optimal value with artificial sweeping is the same as that for PSO algorithm optimization.

To gain further understanding of the high absorption, all these phenomena are discussed with underlying physics by appropriate Fig. 8–10 separately. The absorbed power

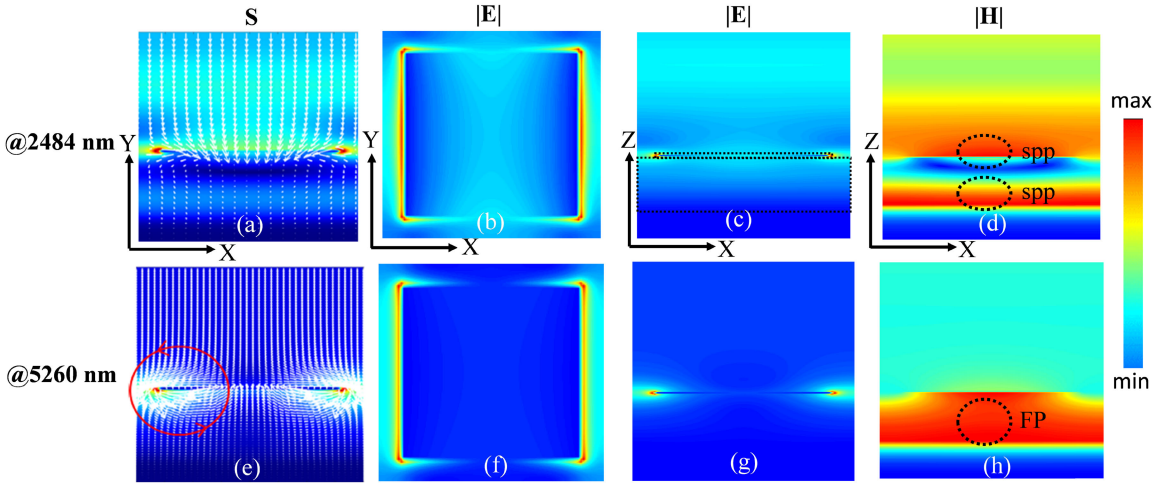

FIGURE 9. (a) and (e) Distributions of energy density and vectors of energy flow (plots of Poynting vector), (b) and (f) distributions of the electric field |E| (color bar in the x-y plane), (c) and (g) distributions of the electric field |E| (color bar in the x-z plane), (d) and (h) magnetic field |H| (color bar in the x-z plane).

distribution ($\boldsymbol{P_{abs}}$) along the x-z plane in Fig. 8 was calculated to gain further understanding of the energy loss in the structure subjected to incident light. Note that the value of $\boldsymbol{P_{abs}}$ for nonmagnetic materials can be obtained by the formula: $\boldsymbol{P_{abs}} = \nabla \cdot \vec{s} = \frac{1}{2}\omega\varepsilon''|\boldsymbol{E}|^2$, where ε'' is the imaginary part of permittivity, ω is the angular frequency, and $|\boldsymbol{E}|$ is the total electric field distribution [29]. As shown in Figs. 8(a) and (b), most power absorption power occurred on top Fe layer, accounting for more than 20-fold loss than that of bottom Fe. As the major absorption layer in the metamaterials absorber, the top Fe layer has a large extinction coefficients, especially in the ATW range. (The infrared optical constants, refractive indexes "n" and extinction coefficients "k" of the Fe layer are presented in Fig. 2(c)). However, the screening effect of a thick metal film keeps the fluctuating currents from the absorber to the free space; thus, the bottom Fe layer contributes little to the absorption of the absorber and behaves as a reflective layer. In addition, when the incident electromagnetic wave is 2484 nm, the loss of the top Fe layer exists mainly in the sides and the middle, while when the incident wavelength is 5260 nm, the loss of the top Fe layer exists mainly in the sides.

To further understand the physical mechanism of this absorber, we also calculate the electric field distribution $|E|$, magnetic field distribution $|H|$, energy density and energy flow vector (Poynting vector S diagram) along the x-z plane at different wavelengths in Fig. 9. The TM-polarized light is vertically incident at different resonance wavelengths of 2484, and 5260 nm.

When the incident electromagnetic wave wavelength is 2484 nm, the absorption rate of the absorber is 98.3%. As shown in Fig. 9(a), electromagnetic waves pass through the top Fe cap into the interior of the cavity and the energy decays rapidly, while another part is localized at the edge of the Fe cap. It can be clearly seen in Figs. 9(b) and (c) that the light was coupled to the edge of the Fe cube and the localized surface plasmon polariton (LSPP) was clearly excited in the absorber. The magnetic field was distributed along the metal-dielectric (MgF_2-Fe and TiO_2-Fe) interface, representing the most direct-viewing manifestation of propagating surface plasmon polariton (SPP) as shown in Fig. 9(d). For that the absorption in this band of 2484 nm is the result of the combinations of the LSPP and SPP.

When the incident electromagnetic wave wavelength is 5260 nm, the absorption rate of the absorber is 99.2%. As shown in Fig. 9(e), the most of energy flow $\vec{S}$ first propagated downwardly along the z-axis in MgF_2 cap region, and then whirled into the Fe square region. These patterns formed vortexes close to nanospace between the two adjacent Fe squares, exactly where the electric field was concentrated. The plots of Poynting vector as typical features of slow-light waveguides 5260 nm were also seen in previously published perfect absorbers [16]. Slow light effect has been defined as the propagation of light at very low group velocity in comparison with light speed in vacuum [36]. The reasons behind such a phenomenon have been well interpreted [37]. For example, He *et al.* designed air-dielectric-metal structures, which could support this kind of vortex mode that propagated very slowly along the slab and even being trapped at critical core thickness [36]. Cui *et al.* used slow light mode to broadband absorbers and provided detailed interpretations of slow light effect [16]. Liang *et al.* employed light trapping mechanism to explain the broadband perfect absorption [38]. One can see from Figs. 9(f) and (g) that the light was coupled to the edge of the Fe cube and the localized surface plasmon polariton (LSPP) was excited in the absorber. Another part of the light passes through the gap of the Fe cube and enters a Fabry–Pérot cavity formed by the MDM structure to trigger the cavity resonance. As shown in Fig. 9(h), the magnetic field was basically localized in the dielectric cavity,

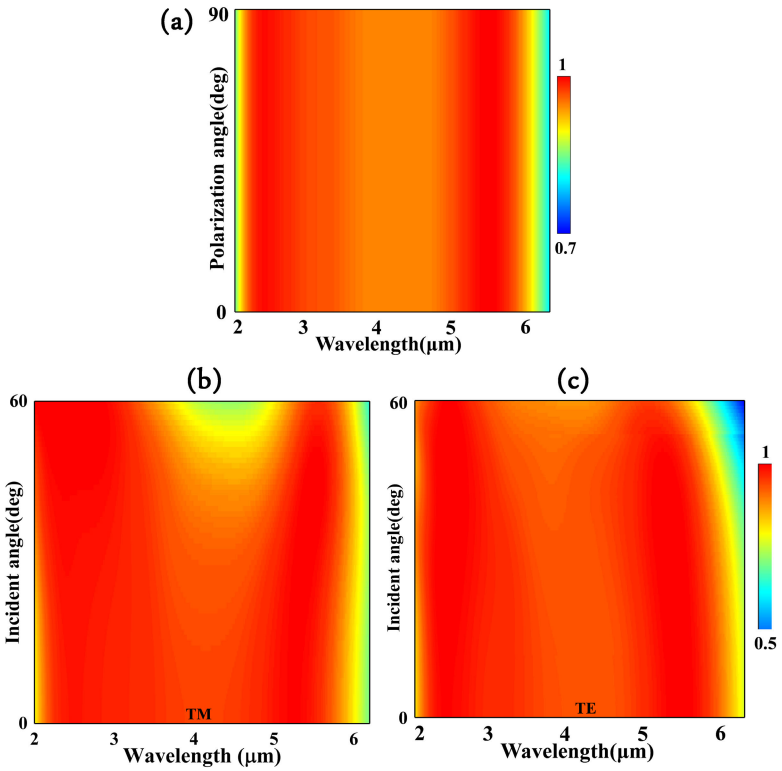

FIGURE 10. Absorption spectra obtained at various polarization angles (a) and incident angles in the (b) TM model and (c) TE model.

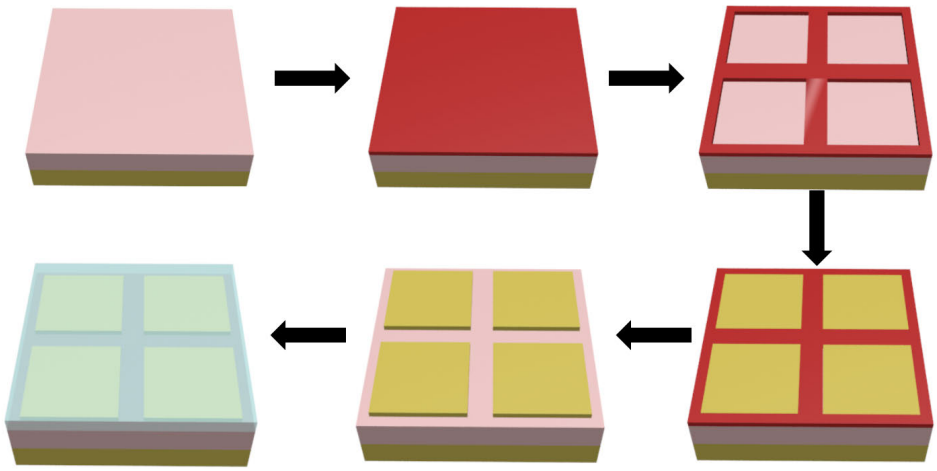

FIGURE 11. The manufacturing process schematic diagram of ATW absorber.

suggesting the contribution of F-P cavity. For that the absorption in this band of 5260 nm is the result of the combinations of the slow light effect, LSPP and F-P cavity.

In the above discussion, an incident TM light was set vertically incident. However, omnidirectional broadband absorption was desirable for many practical applications such as blackbody thermal emitters, remote sensing, and stray light elimination. Thus, the absorption spectra were obtained at different polarization and incidence angles to investigate the angle-dependence and polarization-independent of the proposed absorber. As shown in Fig. 10, the absorber showed polarization-independent features due to the symmetry of the structure. On the other hand, the absorption spectra at oblique incident angles revealed the absorber to maintain high absorption ($>80\%$) in the range of 2000 to 6000 nm under elevated incident angles up to 60°. Previous researches have proved

that the effective permittivity of the overall structure gradually decreases with the increased incident angle, which leads to the blue-shift of absorption range [39], [40]. This indicated an absorber with wide-angle and polarization-independent features [41]–[45].

IV. SIMPLE MANUFACTURING METHOD

A practical preparation method is proposed for this structure. The manufacturing processes are as follows: First, we can use a radio frequency sputtering with dual guns or E-beam to deposit the Fe and TiO_2 layers with the thicknesses of 100 and 270 nm on the surface of Si substrate. Second, polymethyl methacrylate (PMMA) with a thickness of 30 nm is coated on the upper surface of the TiO_2 layer using spin-coating method as the photoresist. Third, we can use electron beam lithography or nano-imprinting lithography to construct the inverse structure of the designed cubes then deposit 10 nm Fe by E-beam. Fourth, a lift-off process is used to move the photoresist off. Finally, a radio frequency sputtering with dual guns or E-beam can be used to deposit the MgF_2 layers with the thicknesses of 600 nm.

V. CONCLUSION

A Earth's ATW metamaterial absorber consisting of simple MDM structure covered by MgF_2 coating was successfully obtained by FDTD methods and optimized by PSO. The proposed absorber exhibited an extremely high average absorption of 96.2% at wavelengths from 2000 nm to 6000 nm corresponding to NIR- and MIR-ATW, respectively. The physical mechanisms of perfect broadband absorption were analysed through hybrid mode of AR effect, LSPR, SPP, F-P cavity, and slow light. The results suggested the broadband ATW absorber to possess simple structure (MDM), higher performance (wide-angle, polarization-independent, and ideal broadband absorption), and low-cost (non-precious metals). Thus, the absorber was suitable for various products of ATW. In sum, the proposed theoretically designed absorber should provide valuable guidelines for future experimental and numerical research dealing with the absorption of ATW.

REFERENCES

[1] C. Zhang, K. Wu, V. Giannini, and X. Li, "Planar hot-electron photodetection with Tamm plasmons," *ACS Nano*, vol. 11, no. 2, pp. 1719–1727, Feb. 2017.
[2] J. Chen, J. Feng, Z. Li, P. Xu, X. Wang, W. Yin, M. Wang, X. Ge, and Y. Yin, "Space-confined seeded growth of black silver nanostructures for solar steam generation," *Nano Lett.*, vol. 19, no. 1, pp. 400–407, 2018.
[3] M. J. Moghimi, G. Lin, and H. Jiang, "Broadband and ultrathin infrared stealth sheets," *Adv. Eng. Mater.*, vol. 20, no. 11, Nov. 2018, Art. no. 1800038.
[4] Y. Qu, Q. Li, L. Cai, M. Pan, P. Ghosh, K. Du, and M. Qiu, "Thermal camouflage based on the phase-changing material GST," *Light, Sci. Appl.*, vol. 7, no. 1, pp. 26–35, Dec. 2018.
[5] A. Hoque and M. T. Islam, "Numerical analysis of single negative broadband metamaterial absorber based on tri thin layer material in visible spectrum for solar cell energy harvesting," *Plasmonics*, vol. 15, no. 4, pp. 1061–1069, Aug. 2020.
[6] M. Faruque, M. Rahman, M. M. Hasan, A. M. Tamim, and M. T. Islam, "Architecture of left-handed metamaterial absorber for absorbing electromagnetic hazards," *J. Optoelectron. Adv. Mater.*, vol. 22, nos. 9–10, pp. 495–500, 2020.
[7] S. Mahmud, S. S. Islam, A. F. Almutairi, and M. T. Islam, "A wide incident angle, ultrathin, polarization-insensitive metamaterial absorber for optical wavelength applications," *IEEE Access*, vol. 8, pp. 129525–129541, 2020.
[8] S. Mahmud, S. S. Islam, K. Mat, M. E. H. Chowdhury, H. Rmili, and M. T. Islam, "Design and parametric analysis of a wide-angle polarization-insensitive metamaterial absorber with a star shape resonator for optical wavelength applications," *Results Phys.*, vol. 18, Sep. 2020, Art. no. 103259.
[9] I. Hossain, M. Samsuzzaman, M. Moniruzzaman, B. B. Bais, M. S. J. Singh, and M. T. Islam, "Polarization-independent broadband optical regime metamaterial absorber for solar harvesting: A numerical approach," *Chin. J. Phys.*, vol. 71, pp. 699–715, Jun. 2021.
[10] N. I. Landy, S. Sajuyigbe, J. J. Mock, D. R. Smith, and W. J. Padilla, "Perfect metamaterial absorber," *Phys. Rev. Lett.*, vol. 100, no. 20, 2008, Art. no. 207402.
[11] H. Deng, Z. Li, L. Stan, D. Rosenmann, D. Czaplewski, J. Gao, and X. Yang, "Broadband perfect absorber based on one ultrathin layer of refractory metal," *Opt. Lett.*, vol. 40, no. 11, pp. 2592–2595, May 2015.
[12] H.-T. Zhou, N. Yu, F. Zou, Z.-H. Yao, G. Gao, and C.-M. Shen, "Controllable preparation of vertically standing graphene sheets and their wettability and supercapacitive properties," *Chin. Phys. B*, vol. 25, no. 9, Sep. 2016, Art. no. 096106.
[13] F. Ding, Y. Cui, X. Ge, Y. Jin, and S. He, "Ultra-broadband microwave metamaterial absorber," *Appl. Phys. Lett.*, vol. 100, no. 10, Mar. 2012, Art. no. 103506.
[14] Z. Liu and K. Aydin, "Localized surface plasmons in nanostructured monolayer black phosphorus," *Nano Lett.*, vol. 16, no. 6, pp. 3457–3462, Jun. 2016.
[15] E. Hecht, *Optics*, 4th ed. New York, NY, USA: Addison Wesley, 2002.
[16] Y. Cui, K. H. Fung, J. Xu, H. Ma, Y. Jin, S. He, and N. X. Fang, "Ultra-broadband light absorption by a sawtooth anisotropic metamaterial slab," *Nano Lett.*, vol. 12, no. 3, pp. 1443–1447, Mar. 2012.
[17] D. Wu, C. Liu, Z. Xu, Y. Liu, Z. Yu, L. Yu, L. Chen, R. Li, R. Ma, and H. Ye, "The design of ultra-broadband selective near-perfect absorber based on photonic structures to achieve near-ideal daytime radiative cooling," *Mater. Des.*, vol. 139, pp. 104–111, Feb. 2018.
[18] W. Yu, Y. Lu, X. Chen, H. Xu, J. Shao, X. Chen, Y. Sun, J. Hao, and N. Dai, "Large-area, broadband, wide-angle plasmonic metasurface absorber for midwavelength infrared atmospheric transparency window," *Adv. Opt. Mater.*, vol. 7, no. 20, Oct. 2019, Art. no. 1900841.
[19] R. Sun, P. Zhou, W. Ai, Y. Liu, Y. Li, R. Jiang, W. Li, X. Weng, L. Bi, and L. Deng, "Broadband switching of mid-infrared atmospheric windows by VO_2-based thermal emitter," *Opt. Exp.*, vol. 27, no. 8, p. 11537, Apr. 2019.
[20] J. Liu, W. Chen, W.-Z. Ma, Y.-S. Chen, X.-C. Deng, P.-P. Zhuang, and Q. Ye, "Biaxial hyperbolic metamaterial THz broadband absorber utilizing anisotropic two-dimensional materials," *Results Phys.*, vol. 22, Mar. 2021, Art. no. 103818.
[21] J. Liu, W. Chen, J.-C. Zheng, Y.-S. Chen, and C.-F. Yang, "Wide-angle polarization-independent ultra-broadband absorber from visible to infrared," *Nanomaterials*, vol. 10, no. 1, p. 27, Dec. 2019.
[22] H. Deng, C. J. Mathai, S. Gangopadhyay, J. Gao, and X. Yang, "Ultra-broadband infrared absorption by tapered hyperbolic multilayer waveguides," *Opt. Exp.*, vol. 26, no. 5, p. 6360, Mar. 2018.
[23] Z. Li, E. Palacios, S. Butun, H. Kocer, and K. Aydin, "Omnidirectional, broadband light absorption using large-area, ultrathin lossy metallic film coatings," *Sci. Rep.*, vol. 5, no. 1, pp. 1–8, Dec. 2015.
[24] W. Chen, J. Liu, W.-Z. Ma, G.-X. Yu, J.-Q. Chen, H.-Y. Cai, and C.-F. Yang, "Numerical study of multilayer planar film structures for ideal absorption in the entire solar spectrum," *Appl. Sci.*, vol. 10, no. 9, p. 3276, May 2020.
[25] C. Yang, C. Ji, W. Shen, K.-T. Lee, Y. Zhang, X. Liu, and L. J. Guo, "Compact multilayer film structures for ultrabroadband, omnidirectional, and efficient absorption," *ACS Photon.*, vol. 3, no. 4, pp. 590–596, Apr. 2016.
[26] P. S. C. Schulze, A. J. Bett, M. Bivour, P. Caprioglio, F. M. Gerspacher, Ö. Ş. Kabakli, A. Richter, M. Stolterfoht, Q. Zhang, D. Neher, M. Hermle, H. Hillebrecht, S. W. Glunz, and J. C. Goldschmidt, "25.1% High-efficiency monolithic perovskite silicon tandem solar cell with a high bandgap perovskite absorber," *Sol. RRL*, vol. 4, no. 7, Jul. 2020, Art. no. 2000152.
[27] W. Ma, F. Cheng, and Y. Liu, "Deep-learning-enabled on-demand design of chiral metamaterials," *ACS Nano*, vol. 12, no. 6, pp. 6326–6334, Jun. 2018.
[28] H. Cai, Y. Sun, X. Wang, and S. Zhan, "Design of an ultra-broadband near-perfect bilayer grating metamaterial absorber based on genetic algorithm," *Opt. Exp.*, vol. 28, no. 10, p. 15347, May 2020.

[29] Z. Tao, J. You, J. Zhang, X. Zheng, H. Liu, and T. Jiang, "Optical circular dichroism engineering in chiral metamaterials utilizing a deep learning network," *Opt. Lett.*, vol. 45, no. 6, p. 1403, Mar. 2020.
[30] L. Peng, D. Liu, H. Cheng, S. Zhou, and M. Zu, "A multilayer film based selective thermal emitter for infrared stealth technology," *Adv. Opt. Mater.*, vol. 6, no. 23, Dec. 2018, Art. no. 1801006.
[31] M. J. Dodge, "Refractive properties of magnesium fluoride," *Applied optics*, vol. 23, no. 12, pp. 1980–1985, 1984.
[32] J. Kischkat, S. Peters, B. Gruska, M. Semtsiv, M. Chashnikova, M. Klinkmüller, O. Fedosenko, S. Machulik, A. Aleksandrova, G. Monastyrskyi, Y. Flores, and W. T. Masselink, "Mid-infrared optical properties of thin films of aluminum oxide, titanium dioxide, silicon dioxide, aluminum nitride, and silicon nitride," *Appl. Opt.*, vol. 51, no. 28, pp. 6789–6798, 2012.
[33] R. C. Weast, *Handbook of Chemistry and Physics*, 55th ed. Boca Raton, FL, USA: CRC Press, 1974.
[34] A. Taflove, *Computational Electromagnetics: The Finite-Difference Time-Domain Method*. Norwood, MA, USA: Artech House, 2005.
[35] K. Aydin, V. E. Ferry, R. M. Briggs, and H. A. Atwater, "Broadband polarization-independent resonant light absorption using ultrathin plasmonic super absorbers," *Nature Commun.*, vol. 2, no. 1, p. 517, Sep. 2011.
[36] S. He, F. Ding, L. Mo, and F. Bao, "Light absorber with an ultra-broad flat band based on multi-sized slow-wave hyperbolic metamaterial thin-films (invited paper)," *Prog. Electromagn. Res.*, vol. 147, pp. 69–79, Jun. 2014.
[37] J. He and S. He, "Slow propagation of electromagnetic waves in a dielectric slab waveguide with a left-handed material substrate," *IEEE Microw. Wireless Compon. Lett.*, vol. 16, no. 2, pp. 96–98, Feb. 2006.
[38] Q. Liang, T. Wang, Z. Lu, Q. Sun, Y. Fu, and W. Yu, "Metamaterial-based two dimensional plasmonic subwavelength structures offer the broadest waveband light harvesting," *Adv. Opt. Mater.*, vol. 1, no. 1, pp. 43–49, Jan. 2013.
[39] R. Feng, J. Qiu, Y. Cao, L. Liu, W. Ding, and L. Chen, "Wide-angle and polarization independent perfect absorber based on one-dimensional fabrication-tolerant stacked array," *Opt. Exp.*, vol. 23, no. 16, pp. 21023–21031, 2015.
[40] G. Zheng, J. Cong, L. Xu, and W. Su, "Angle-insensitive and narrow band grating filter with a gradient-index layer," *Opt. Lett.*, vol. 39, no. 20, pp. 5929–5932, 2014.
[41] F. Ding, Y. Jin, B. Li, H. Cheng, L. Mo, and S. He, "Ultrabroadband strong light absorption based on thin multilayered metamaterials," *Laser Photon. Rev.*, vol. 8, no. 6, pp. 946–953, Nov. 2014.
[42] W. Guo, Y. Liu, and T. Han, "Ultra-broadband infrared metasurface absorber," *Opt. Exp.*, vol. 24, no. 18, p. 20586, Sep. 2016.
[43] F. Ding, J. Dai, Y. Chen, J. Zhu, Y. Jin, and S. I. Bozhevolnyi, "Broadband near-infrared metamaterial absorbers utilizing highly lossy metals," *Sci. Rep.*, vol. 6, no. 1, pp. 1–9, Dec. 2016.
[44] F. Ding, Y. Yang, R. A. Deshpande, and S. I. Bozhevolnyi, "A review of gap-surface plasmon metasurfaces: Fundamentals and applications," *Nanophotonics*, vol. 7, no. 6, pp. 1129–1156, Jun. 2018.
[45] Y. Li, Z. Liu, H. Zhang, P. Tang, B. Wu, and G. Liu, "Ultra-broadband perfect absorber utilizing refractory materials in metal-insulator composite multilayer stacks," *Opt. Exp.*, vol. 27, no. 8, p. 11809, Apr. 2019.
[46] Y. Li, L. Li, F. Wang, H. Ge, R. Xie, and B. An, "Two broad absorption bands in infrared atmosphere transparent windows by trapezoid multilayered grating," *Opt. Mater. Exp.*, vol. 10, no. 2, p. 682, 2020.
[47] A. Tittl, A.-K.-U. Michel, M. Schäferling, X. Yin, B. Gholipour, L. Cui, M. Wuttig, T. Taubner, F. Neubrech, and H. Giessen, "A switchable mid-infrared plasmonic perfect absorber with multispectral thermal imaging capability," *Adv. Mater.*, vol. 27, no. 31, pp. 4597–4603, Aug. 2015.

JING LIU received the B.S. and M.S. degrees from Fujian Normal University, China, in 2004 and 2007, respectively, and the Ph.D. degree from Xiamen University, China, in 2014. From 2007 to 2014, he was an Assistant Professor with Jimei University, China. Since 2015, he has been an Associate Professor with Jimei University. Since 2019, he has been an Associate Professor with Jimei University. His research interests include nanomaterials and absorbers.

WEN-ZHUANG MA was born in Weifang, Shandong, China, in 1997. He received the B.S. degree in information engineering from Ludong University, Yantai, in 2019. He is currently pursuing the M.S. degree with Jimei University, Fujian, China.

His research interests include metamaterial and broadband absorber, and localized surface plasmon resonance.

WEI CHEN was born in Taizhou, Jiangsu, China, in 1995. He received the B.S. degree in electronic science and technology from Changzhou University, Changzhou, in 2018. He is currently pursuing the M.S. degree with Jimei University, Fujian, China.

His research interests include metamaterial and broadband absorber, and localized surface plasmon resonance.

YU-SHAN CHEN was born in Fujian, China in 1983. She received the B.S. and M.S. degrees from the College of Information Science and Engineering, Huaqiao University, in 2004 and 2007, and the Ph.D. degree from the School of Informatics, Xiamen University, in 2013. From 2007 to 2009, she was a Lecturer with the Xiamen University Tan Kah Kee College. Since 2013, she has been an Assistant Professor with the Information Engineering College, Jimei University. Her research interests include optical sensors and surface plasmon resonance of nanoparticles.

XU-CHU DENG was born in Xiamen, China, in 1986. He received the B.S. degree from the Nanjing University of Posts and Telecommunications, in 2004, and the Ph.D. degree from Xiamen University, in 2015. From 2013 to 2015, he was a Visiting Fellow with the Pacific Northwest National Laboratory, USA. Since 2019, he has been an Assistant Professor with the Information Engineering College, Jimei University. His research interests include optical sensors and absorbers.

YU GU received the B.S. degree in civil and building engineering and the M.S. and Ph.D. degrees in solid mechanics from the Belarusian State University of Transport, Belarus, in 1999, 2001, and 2006, respectively. He is currently a Professor with the School of Information Engineering, Jimei University. He is also a Professor with the Department of Chemistry, Goethe-University Frankfurt. His research interests include pattern recognition, the design and preparation of multi-functional advanced materials for biochemical sensors, computational intelligence self-adaptive systems, and the theory of solid mechanics.